Earthq Eng & Eng Vib (2025) 24: 15-30 **DOI**: https://10.1007/s11803-025-2292-x

An efficient conversion model between acceleration and pseudo-acceleration response spectra considering effects of magnitude, distance, and site class

Liu Zheng[1†], Zhao Yan-Gang[1‡] and Zhang Haizhong[2§]

1. *Key Laboratory of Urban Security and Disaster Engineering of Ministry of Education, Beijing University of Technology, Beijing 100124, China*
2. *Faculty of Agriculture,Yamagata University, 1-23, Wakaba-machi, Tsuruoka-shi, Yamagata 997-8555, Japan*

Abstract: Both acceleration and pseudo-acceleration response spectra play important roles in structural seismic design. However, only one of them is generally provided in most seismic codes. Therefore, many studies have attempted to develop conversion models between the acceleration response spectrum (*SA*) and the pseudo-acceleration response spectrum (*PSA*). Our previous studies found that the relationship between *SA* and *PSA* is affected by magnitude, distance, and site class. Subsequently, we developed an *SA*/*PSA* model incorporating these effects. However, this model is suitable for cases with small and moderate magnitudes and its accuracy is not good enough for cases with large magnitudes. This paper aims to develop an efficient *SA*/*PSA* model by considering influences of magnitude, distance, and site class, which can be applied to cases not only with small or moderate magnitudes but also with large ones. For this purpose, regression analyses were conducted using 16,660 horizontal seismic records with a wider range of magnitude. The magnitude of these seismic records varies from 4 to 9 and the distances vary from 10 to 200 km. These ground motions were recorded at 338 stations covering four site classes. By comparing them with existing models, it was found that the proposed model shows better accuracy for cases with any magnitudes, distances, and site classes considered in this study.

Keywords: acceleration response spectrum; pseudo-acceleration response spectrum; magnitude; distance; site class

1 Introduction

Both acceleration and pseudo-acceleration response spectra play important roles in structural seismic design. The acceleration response spectrum (*SA*) is suitable for cases in which inertial force is of interest in seismic design, e.g., for the design of a structural foundation, while the pseudo-acceleration response spectrum (*PSA*) is suitable for cases in which either the restoring force or the relative displacement are of interest in the seismic design, e.g., in the design of the superstructures of regular buildings and buildings with energy dissipation devices (Lin and Chang, 2003). However, although both *SA* and *PSA* can be calculated directly using time histories, most seismic codes only provide either *SA* and *PSA* as the seismic load and do not include time histories. For example, the Chinese seismic code (GB 50010-2010, 2016) and the Japanese Building Standard (BSL, 2005) provide *SA*, while Eurocode 8 (2004) and ASCE/SEI7-16 (2016) provide *PSA*. Although *SA* is almost the same as *PSA* at small damping ratios, both can be significantly different at large damping ratios, e.g., for seismic isolation systems and structures equipped with energy dissipation devices (Jenschke *et al*., 1964, 1965; Veletsos and Newmark, 1964; Newmark and Rosenblueth, 1971; Boore, 2001; Chopra, 2007). The use of *SA* and *PSA* interchangeably at large damping ratios can have negative implications on seismic design, specifically, estimating the restoring force with *SA* instead of *PSA* would render the design too conservative, and estimating the inertial force with *PSA* instead of *SA* would make the design force too small (Zhang and Zhao, 2022b).

Therefore, many studies have worked to elucidate the relationship between *SA* and *PSA* and have developed conversion models that lie between *SA* and *PSA*. Sadek *et al*. (2000) discussed the relationship between *SA* and *PSA* based on the regression analysis of 72 horizontal seismic records from 36 stations in the western United States and proposed a conversion model falling between *SA* and *PSA*. Song *et al*. (2007) proposed an analytical model between *SA* and *PSA* based on the assumption that earthquake excitation is a Gaussian stationary process.

Correspondence to: Zhang Haizhong, Faculty of Agriculture, Yamagata University, 1-23, Wakaba-machi, Tsuruoka-shi, Yamagata 997-8555, Japan
Tel.: +81-0235-28-2945
Email: zhang@tds1.tr.yamagata-u.ac.jp
[†]PhD Candidate; [‡]Professor; [§]Associate Professor

Supported by: National Natural Science Foundation of China under Grant No. 52278135
Received January 6, 2024; **Accepted** August 5, 2024

Mentrasti (2008) theoretically analyzed and explained the relationship between *SA* and *PSA* based on an exact integral analysis and proposed a conversion model between *SA* and *PSA*. Papagiannopoulos *et al*. (2013) proposed a conversion model between *SA* and *PSA*, based on a regression analysis of 866 horizontal seismic records grouped by magnitude, distance, and site class. Zhang *et al*. (2016) discussed the differences between *SA* and *PSA* and compared the differences at different damping ratios, based on the El Centro seismic record.

Most of the above models for the relationship between *SA* and *PSA* incorporate the structural period and damping ratio as input parameters. Our previous studies (Hang *et al*., 2022; Zhang and Zhao, 2022b) found that the relationship between *SA* and *PSA* is also affected by magnitude, distance, and site class. Hang *et al*. (2022) explored influences of magnitude, distance, and site class on the relationship between *SA* and *PSA* based on statistical analyses of 16,660 seismic acceleration time histories, and established a conversion model between *SA* and *PSA* that directly contained these seismic parameters as input parameters. Since magnitude and distance are not available in seismic codes, this model (Hang *et al*., 2022) cannot be directly applied to seismic design. Zhang and Zhao (2022b) used a response-spectrum-shape factor to reflect influences of magnitude and distance and proposed a model incorporating this shape factor, which can be directly applied in seismic design. However, this model is suitable for cases with small or moderate magnitudes, and therefore its accuracy is not sufficient for cases with large magnitudes.

The purpose of this study is to develop an efficient *SA*/*PSA* model by considering influences of magnitude, distance, and site class, which can be applied to cases not only with small and moderate magnitudes but also with large magnitudes. The remainder of the paper is organized as follows. In Section 2, existing conversion models between *SA* and *PSA* are reviewed. In Section 3, 16,660 horizontal seismic records that cover a wide range of magnitude were selected from the strong-motion seismograph networks (K-NET, KIK-net) of Japan. In Section 4, we report on regression analyses that used selected records and were conducted to develop an *SA*/*PSA* model incorporating effects of magnitude, distance, and site class. In Section 5, the results of the proposed model are compared with those of existing models. In Section 6, the results of this article are summarized.

2 Literature review

Sadek *et al*. (2000) discussed the relationship between *SA* and *PSA* based on regression analyses of 72 horizontal seismic records from 36 stations in the western United States and proposed a conversion model between *SA* and *PSA*. This model considers a period range of 0.1 s to 4 s and damping ratios of 2%, 5%, 10%, 15%, 20%, 30%, 40%, 50%, and 60%, which is expressed as:

$$\frac{SA}{PSA}=1+2.436\xi^{1.895}T^{(0.628+0.205\xi)} \tag{1}$$

in which ξ and T are the damping ratio and the structural period, respectively.

Song *et al*. (2007) proposed an analytical model between *SA* and *PSA* based on the assumption that the earthquake excitation is a Gaussian stationary process. This model is expressed as follows:

$$\frac{SA}{PSA}=\sqrt{1+4\xi^2} \tag{2}$$

Mentrasti (2008) theoretically analyzed and explained the relationship between *SA* and *PSA* based on an exact integral analysis and proposed a conversion model between *SA* and *PSA*. This model is suitable for cases with a structural period from 0 s to 6 s, which is expressed as:

$$\frac{SA}{PSA}=\frac{1+2\xi^2}{1+2\xi^2\exp\left(-1.8T\right)} \tag{3}$$

Papagiannopoulos *et al*. (2013) proposed a conversion model between *SA* and *PSA* based on 866 seismic acceleration time histories (two horizontal components of 433 acceleration records), which were organized into 20 groups according to magnitude, distance, and site class. This model considers structural periods from 0 s to 5 s and damping ratios of 5%, 8%, 10%, 15%, 20%, 25%, 30%, 40%, and 50%, which is expressed as:

$$\frac{SA}{PSA}=o_1+o_2T+o_3\xi+o_4T^2+o_5\xi^2+o_6\xi T \tag{4}$$

where o_1–o_6 are regression coefficients, which are listed in Table 5 of Papagiannopoulos *et al*. (2013).

Hang *et al*. (2022) systematically analyzed influences of magnitude, distance, and site class on the relationship between *SA* and *PSA* based on statistical analysis of 16,660 seismic acceleration time histories, and established a conversion model between *SA* and *PSA* containing these seismic parameters as input parameters. This model considers the structural period from 0.01 s to 10 s and damping ratios of 5%, 10%, 20%, 30%, 40%, and 50%, which is expressed as:

$$\frac{SA}{PSA}=1+k_1\xi^{k_2}T^{k_3} \tag{5}$$

where $k_1 - k_3$ are regression coefficients which can be obtained from Table 2 of Hang *et al*. (2022).

Since magnitude and distance are not available in seismic codes, the Hang model (Hang *et al*., 2022) cannot be directly applied to seismic design. Zhang and Zhao (2022b) used a response-spectrum-shape factor to reflect influences of magnitude and distance and proposed a model incorporating this shape factor, which can be directly applied in seismic design. This model considers structural periods from 0.01 s to 10 s and damping ratios of 10% to 50%, which is expressed as:

$$\frac{SA}{PSA} = 1 + \left(0.14\xi^{1.54}\zeta_{PSA}{}^{-0.57}\right)T^{\xi^{-0.2}/\left(5\sqrt{\zeta_{PSA}}+1\right)} \tag{6}$$

in which ζ_{PSA} is the response-spectrum-shape factor obtained from the *PSA*, which is expressed as:

$$\zeta_{PSA} = \frac{PSA(6\text{ s})}{PGA} \tag{7}$$

in which *PSA* (6 s) is the value of 5%-damped *PSA* at 6 s, and *PGA* is peak ground acceleration (i.e., *PSA* at 0 s). However, the model proposed by Zhang and Zhao (2022b) is suitable for cases with small or moderate magnitudes, but its accuracy is not sufficient for cases with large magnitudes. The purpose of this study is to develop an efficient *SA*/*PSA* model by considering influences of magnitude, distance, and site class, which can be applied to cases not only with small or moderate magnitudes but also with large magnitudes.

3 Ground motion databases

To establish an *SA*/*PSA* model that is suitable for a wide range of magnitudes, a total of 16,660 horizontal seismic records covering a wide range of magnitude (*M*), distance (*R*), and site classes were collected from strong-motion seismograph networks, K-NET, KiK-net (Okada *et al*., 2004; Aoi *et al*., 2011; Zhang *et al*., 2023). The magnitude of these selected records varies from 4 to 9 and the distance varies from 10 to 200 km. The selected ground motions were recorded at 338 stations, which can be divided into four site classes (B, C, D, and E) based on an average shear-wave velocity in the upper 30 m ($\overline{v}_{s30}$), as specified by the National Earthquake Hazards Reduction Program (NEHRP, 2000). This paper does not include site class A because there are few sites belonging to this site class in K-NET and KiK-net. The shear-wave velocity provided by the KiK-net network is greater than 30 m, and thus, $\overline{v}_{s30}$ can be obtained directly. However, K-NET provides a shear-wave velocity in the upper 20 m ($\overline{v}_{s20}$) only. To determine the $\overline{v}_{s30}$ values of the K-NET network, the formula proposed by Kanno *et al*. (2006) is employed to derive $\overline{v}_{s30}$ from $\overline{v}_{s20}$. The distributions of magnitude *M* and distance *R* for the four classes are shown in Fig. 1. There are many criteria for defining near-fault motions (Chopra and Chintanapakdee, 2001; Hatzigeorgiou, 2010; Seyed Ardakani *et al*., 2021; Stewart *et al*., 2002; Fu *et al*., 2023), according to the criterion adopted by Hatzigeorgiou (2010), 98% of the records used in this study are classified as far-field $R \in [20\text{ km}, +\infty)$, with no near-fault $R \in [0\text{ km}, 10\text{ km}]$ motions included, and 2% of the records fall in between. Therefore, this study did not consider the effects of near-fault seismic motions.

The collected records in each site class are divided into three groups based on magnitude $M \in [4, 5.5)$,

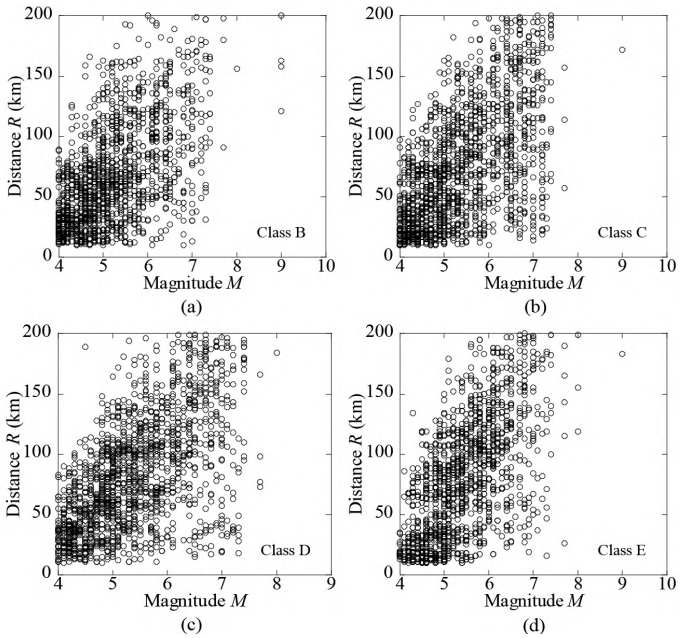

Fig. 1 Distribution of magnitude *M* and distance *R*

$M \in [5.5, 6.5)$, and $M \in [6.5, +\infty)$. Each group is further divided into three subgroups based on the distance $R \in [10\text{ km}, 50\text{ km})$, $R \in [50\text{ km}, 100\text{ km})$, and $R \in [100\text{ km}, 200\text{ km}]$, as listed in Table 1. The above earthquake database was constructed using ground motions recorded from 1996 to 2020 to establish an *SA*/*PSA* conversion model. To comprehensively confirm the performance of the established conversion model, an additional earthquake database, using ground motions recorded from 2021 to 2024, was selected based on the same criteria described above and as listed in Table 2. This additional database consists of 15,722 ground motion records.

Additionally, a baseline adjustment is applied to all records to remove long-period noise. Ideally, each

Table 1 Classification of ground-motion database for model construction according to magnitude, distance, and site class

Magnitude, M	Distance, R (km)	Record count	Group	Site class
$M \in [4, 5.5)$	$R \in [10, 50)$	1102	1	B
	$R \in [50, 100)$	700	2	
	$R \in [100, 200]$	196	3	
$M \in [5.5, 6.5)$	$R \in [10, 50)$	142	4	
	$R \in [50, 100)$	298	5	
	$R \in [100, 200]$	274	6	
$M \in [6.5, +\infty)$	$R \in [10, 50)$	40	7	
	$R \in [50, 100)$	102	8	
	$R \in [100, 200]$	178	9	
$M \in [4, 5.5)$	$R \in [10, 50)$	1326	10	C
	$R \in [50, 100)$	978	11	
	$R \in [100, 200]$	272	12	
$M \in [5.5, 6.5)$	$R \in [10, 50)$	164	13	
	$R \in [50, 100)$	384	14	
	$R \in [100, 200]$	470	15	
$M \in [6.5, +\infty)$	$R \in [10, 50)$	102	16	
	$R \in [50, 100)$	176	17	
	$R \in [100, 200]$	412	18	
$M \in [4, 5.5)$	$R \in [10, 50)$	1606	19	D
	$R \in [50, 100)$	1566	20	
	$R \in [100, 200]$	706	21	
$M \in [5.5, 6.5)$	$R \in [10, 50)$	194	22	
	$R \in [50, 100)$	568	23	
	$R \in [100, 200]$	1046	24	
$M \in [6.5, +\infty)$	$R \in [10, 50)$	104	25	
	$R \in [50, 100)$	116	26	
	$R \in [100, 200]$	512	27	
$M \in [4, 5.5)$	$R \in [10, 50)$	828	28	E
	$R \in [50, 100)$	594	29	
	$R \in [100, 200]$	206	30	
$M \in [5.5, 6.5)$	$R \in [10, 50)$	124	31	
	$R \in [50, 100)$	278	32	
	$R \in [100, 200]$	542	33	
$M \in [6.5, +\infty)$	$R \in [10, 50)$	38	34	
	$R \in [50, 100)$	68	35	
	$R \in [100, 200]$	248	36	
		16660	36	

Table 2 Classification of ground-motion database for model validation according to magnitude, distance, and site class

Magnitude, M	Distance, R (km)	Record count	Group	Site class
$M \in [4, 5.5)$	$R \in [10, 50)$	314	1	B
	$R \in [50, 100)$	252	2	
	$R \in [100, 200]$	20	3	
$M \in [5.5, 6.5)$	$R \in [10, 50)$	26	4	
	$R \in [50, 100)$	62	5	
	$R \in [100, 200]$	48	6	
$M \in [6.5, +\infty)$	$R \in [10, 50)$	20	7	
	$R \in [50, 100)$	48	8	
	$R \in [100, 200]$	56	9	
$M \in [4, 5.5)$	$R \in [10, 50)$	2098	10	C
	$R \in [50, 100)$	1926	11	
	$R \in [100, 200]$	568	12	
$M \in [5.5, 6.5)$	$R \in [10, 50)$	160	13	
	$R \in [50, 100)$	414	14	
	$R \in [100, 200]$	666	15	
$M \in [6.5, +\infty)$	$R \in [10, 50)$	48	16	
	$R \in [50, 100)$	220	17	
	$R \in [100, 200]$	706	18	
$M \in [4, 5.5)$	$R \in [10, 50)$	2306	19	D
	$R \in [50, 100)$	2220	20	
	$R \in [100, 200]$	564	21	
$M \in [5.5, 6.5)$	$R \in [10, 50)$	178	22	
	$R \in [50, 100)$	510	23	
	$R \in [100, 200]$	766	24	
$M \in [6.5, +\infty)$	$R \in [10, 50)$	26	25	
	$R \in [50, 100)$	146	26	
	$R \in [100, 200]$	554	27	
$M \in [4, 5.5)$	$R \in [10, 50)$	334	28	E
	$R \in [50, 100)$	142	29	
	$R \in [100, 200]$	40	30	
$M \in [5.5, 6.5)$	$R \in [10, 50)$	30	31	
	$R \in [50, 100)$	90	32	
	$R \in [100, 200]$	78	33	
$M \in [6.5, +\infty)$	$R \in [10, 50)$	4	34	
	$R \in [50, 100)$	26	35	
	$R \in [100, 200]$	56	36	
		15722	36	

ground motion record should also be processed to filter out frequencies with unacceptable low signal-to-noise ratios and should be used only within the available frequency range. However, since this study focuses on the *SA*/*PSA* ratio, it is assumed that the noise present in both *SA* and *PSA* can be negated through the calculation of this ratio. To validate this assumption, a comparison was made between the *SA*/*PSA* results with and without processing the ground motion records, as shown in Fig. 2. The group with the smallest magnitudes $M \in [4, 5.5)$ and the largest distances $R \in [100\,\text{km}, 200\,\text{km}]$ in site class C, which may be mostly affected by noise, were selected for the comparison. The automatic P-phase arrival-time picker developed by Kalkan (2016) was used to identify the noise window, and the method devised by Bahrampouri *et al*. (2021) was employed to filter out frequencies with unacceptable low signal-to-noise ratios. As observed in Fig. 2, there is no significant

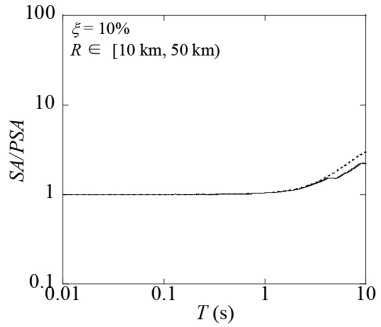

Fig. 2 Comparison between the *SA*/*PSA* results with and without processing the ground motion records. The solid lines represent the results with processing the ground motion records; the dashed lines represent the results without processing the ground motion records

difference between the *SA*/*PSA* results with and without the ground motion records being processed, especially within the first six seconds, which is of particular interest in engineering. The average relative difference between the two within this period is only 7.2%. Thus, filtering out frequencies with unacceptable low signal-to-noise ratios has no significant impact on the *SA*/*PSA* ratio. Consequently, ground motion records were not processed further, except for the baseline adjustment.

4 Proposed *SA*/*PSA* model

To develop an *SA*/*PSA* model that can be applied to a wide range of magnitude, many *SA*/*PSA* function forms are employed, based on regression analyses of the selected ground motion records. Considering the balance between accuracy and simplicity, an *SA*/*PSA* model is proposed as:

$$\frac{SA}{PSA}=1+aT^{b} \tag{8}$$

where a and b are the regression coefficients. It can be known from Eq. (8) that when T = 0, *SA*/*PSA* = 1, the proposed model satisfies the boundary conditions.

Since a and b vary with magnitude, distance, and site class, a and b can be regressed as a function according to the response-spectrum-shape factor (ζ_{PSA}) obtained from *PSA* as proposed by Zhang and Zhao (2022a) as:

$$a=\exp\begin{pmatrix}\left(m_1+m_2\ln\xi+m_3/\xi\right)+\left(m_4+m_5\ln\xi+m_6/\xi\right)/\zeta_{PSA}+\\ \left(m_7+m_8\xi^2+m_9/\ln\xi\right)^{-1}/\zeta_{PSA}{}^{0.5}\end{pmatrix} \tag{9}$$

$$b=\left(n_1+n_2\ln\xi+n_3\ln\zeta_{PSA}\right)/\left(1+n_4\ln\xi+n_5\ln\zeta_{PSA}+n_6\left(\ln\zeta_{PSA}\right)^2\right) \tag{10}$$

where m_1–m_9 and n_1–n_6 are coefficients regressed nonlinearly based on the least squares method, as listed in Table 3.

The above parameters a and b are expressed using Eqs. (9) and (10) and are used to obtain *SA* from a given *PSA*. When the *PSA* must be obtained from a given *SA*, the parameters a and b are estimated by the following equations:

$$a=\exp\begin{pmatrix}\left(m_1+m_2\ln\xi+m_3/\xi\right)+\left(m_4+m_5\ln\xi+m_6/\xi\right)/\zeta_{SA}\\ +\left(m_7+m_8\xi^2+m_9/\ln\xi\right)^{-1}/\zeta_{SA}{}^{0.5}\end{pmatrix} \tag{11}$$

$$b=\left(n_1+n_2\ln\xi+n_3\ln\zeta_{SA}\right)/\left(1+n_4\ln\xi+n_5\ln\zeta_{SA}+n_6\left(\ln\zeta_{SA}\right)^2\right) \tag{12}$$

where m_1–m_9 and n_1–n_6 are coefficients regressed nonlinearly based on the least squares method, as listed in Table 4. Since only the *SA* is given when using Eqs. (11) and (12) to obtain *PSA*, the response-spectrum-shape factor ζ_{SA} is defined according to the *SA*, which is expressed as:

$$\zeta_{SA}=\frac{SA(6\text{ s})}{PGA} \tag{13}$$

in which *SA* (6 s) is the value of *SA* at 6 s.

Figures 3–5 compare the *SA*/*PSA* results obtained using the proposed model, with those obtained results using the ground-motion database for model construction (Table 1) for damping ratios of 10%, 30%, and 50%, respectively. It can be found that the *SA*/*PSA* results obtained using the proposed model have a high degree of accuracy compared with those of the seismic

Table 3 Values of regression coefficients in Eqs. (9) and (10)

	B	C	D	E
m_1	1.392559	1.228452	1.347829	1.025926
m_2	1.632358	2.684166	2.397859	2.193939
m_3	–0.04502	–0.05912	–0.17397	–0.17656
m_4	0.000944	0.000503	0.001962	0.00507
m_5	–0.00099	0.002457	0.002102	0.000538
m_6	0.0000331	–0.0000115	–0.00048	–0.00094
m_7	–3.48258	–0.40942	–1.86858	–2.66321
m_8	–337.229	–11.8387	–7.88307	4.095474
m_9	55.05638	–8.79314	–10.716	–12.9916
n_1	–0.4752	–0.4376	–0.4509	0.1521
n_2	–0.0081	–0.1195	–0.1134	–0.07502
n_3	–0.1929	–0.2463	–0.287	–0.09279
n_4	0.09729	0.09075	0.1235	0.06963
n_5	0.2603	0.1987	0.1954	0.2751
n_6	0.03946	0.04201	0.04544	0.04345

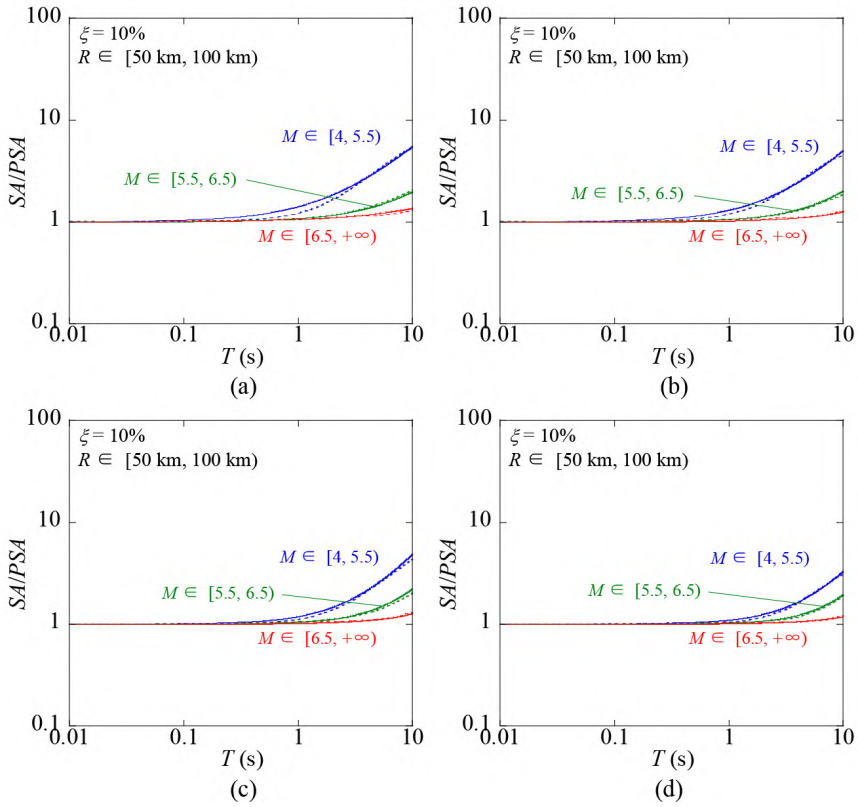

Fig. 3 Comparison of the *SA*/*PSA* results obtained by the proposed model and those obtained using the ground-motion database for model construction considering a damping ratio of 10% for (a) class B, (b) class C, (c) class D, and (d) class E. The solid lines represent the results from the proposed approach; the dashed lines represent the results from actual ground motion record

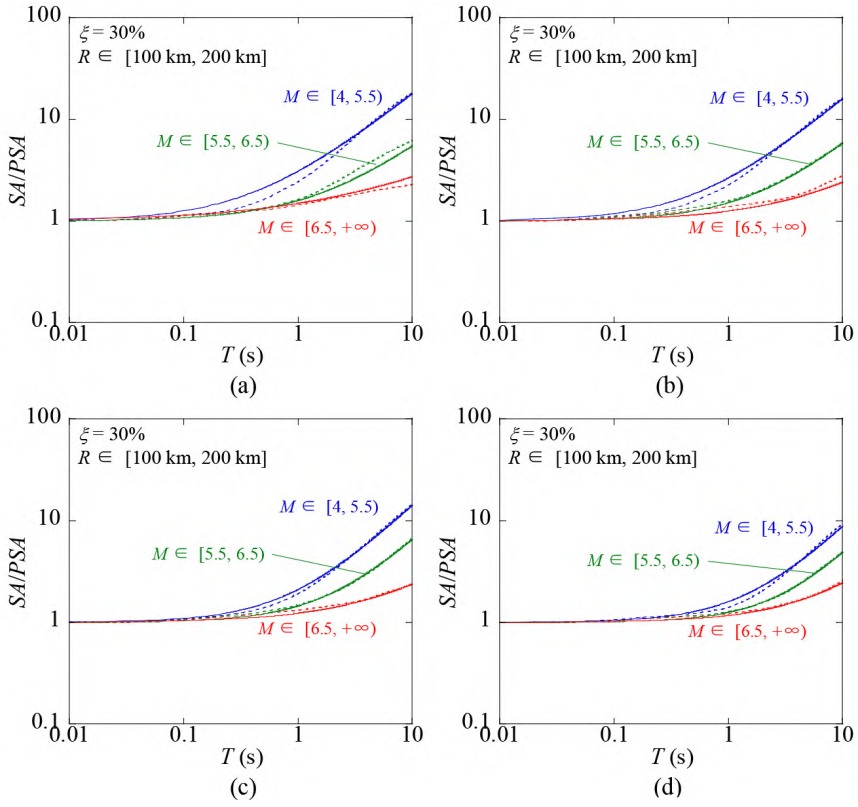

Fig. 4 Comparison of the *SA*/*PSA* results obtained by the proposed model and those obtained using the ground-motion database for model construction considering a damping ratio of 30% for (a) class B, (b) class C, (c) class D, and (d) class E. The solid lines represent the results from the proposed approach; the dashed lines represent the results from actual ground motion records

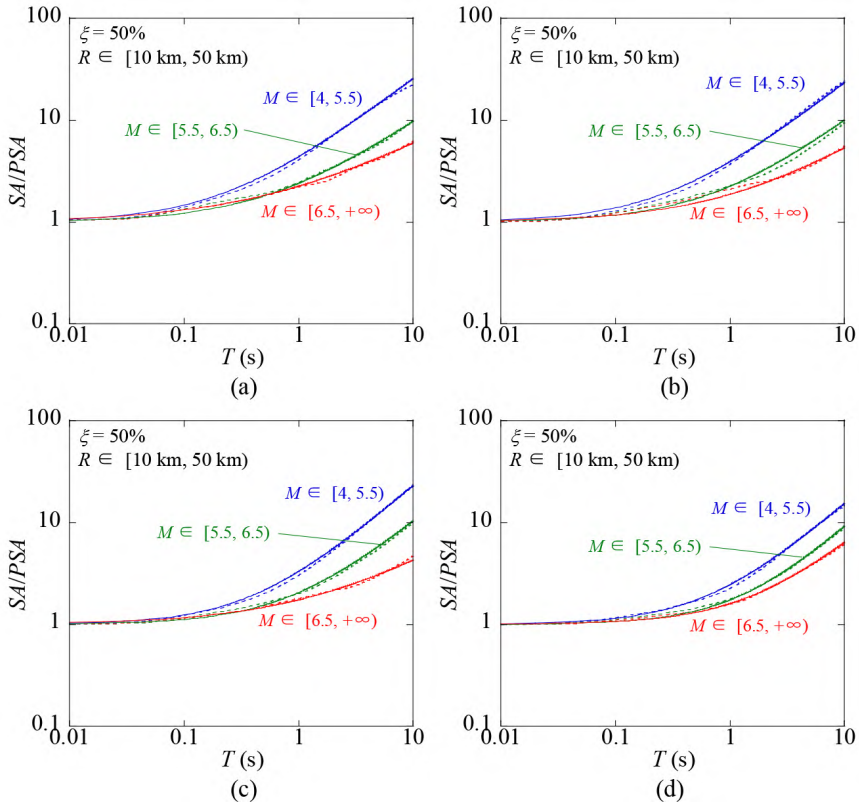

Fig. 5 Comparison of the *SA*/*PSA* results obtained by the proposed model and those obtained using the ground-motion database for model construction considering a damping ratio of 50% for (a) class B, (b) class C, (c) class D, and (d) class E. The solid lines represent the results from the proposed approach; the dashed lines represent the results from actual ground motion records

Table 4 Values of regression coefficients in Eqs. (11) and (12)

	B	C	D	E
m_1	1.1066513	1.6100658	1.3743777	1.1350511
m_2	1.5352226	3.1560363	2.0620713	2.3529145
m_3	–0.066589588	–0.1351325	–0.28374776	–0.18295765
m_4	0.00260686	0.00530585	0.005459775	0.008598546
m_5	–0.00159397	0.00695293	–0.00058141	0.001266024
m_6	0.000121041	–0.000331901	–0.001582609	–0.001309912
m_7	–3.4825829	–0.4285301	–2.2150934	–1.6602839
m_8	–337.2288	6.5711015	16.038387	20.294283
m_9	55.056384	–4.7745082	–9.9940419	–8.8582606
n_1	–0.7714	–0.3255	–0.4699	0.09017
n_2	0.05987	–0.06341	–0.09425	–0.08728
n_3	–0.2642	–0.1829	–0.2792	–0.1269
n_4	0.1309	0.07214	0.1089	0.07798
n_5	0.3952	0.2961	0.2602	0.2724
n_6	0.06556	0.04944	0.05528	0.04879

records, and accuracy increases with an increase in magnitude. The average relative errors incurred by use of the proposed model in the periods of 0.01–10 s are applied to quantify its accuracy. The maximum average relative errors are limited to 15% and 3.6% for site class B and site class E, respectively, while the minimum value is only 0.005% and 0.03%, respectively. For the case shown in Fig. 3, when the magnitude varies from [4, 5.5) to [6.5, +∞), the average relative error decreases from 2.38% to 2.06% in site class B, while the average relative error decreases from 3.58% to 1.95% in site class E. Moreover, the accuracy of the proposed model increases as the site class varies from B to E. For the case of $M \in [4, 5.5)$ as displayed in Fig. 5, when the site class varies from B to E, the average relative error by the proposed model decreases from 10% to 0.4%. Similar trends are observed for the results not shown here, such as those of damping ratios of 5%, 20%, and 40%. Additionally, considering the effect of noise, it is advised to apply the proposed *SA*/*PSA* model within the first six seconds. Moreover, since the *SA*/*PSA* model was developed based on seismic data taken from Japan, its applicability is currently limited to this region. Its suitability for other regions has not been discussed in this paper and requires further study in future work.

To comprehensively confirm the performance of the proposed conversion model, the evaluated *SA*/*PSA* results were also compared with those obtained by using the ground-motion database for model validation (Table 2), as shown in Figs. 6–8. The overall consistency

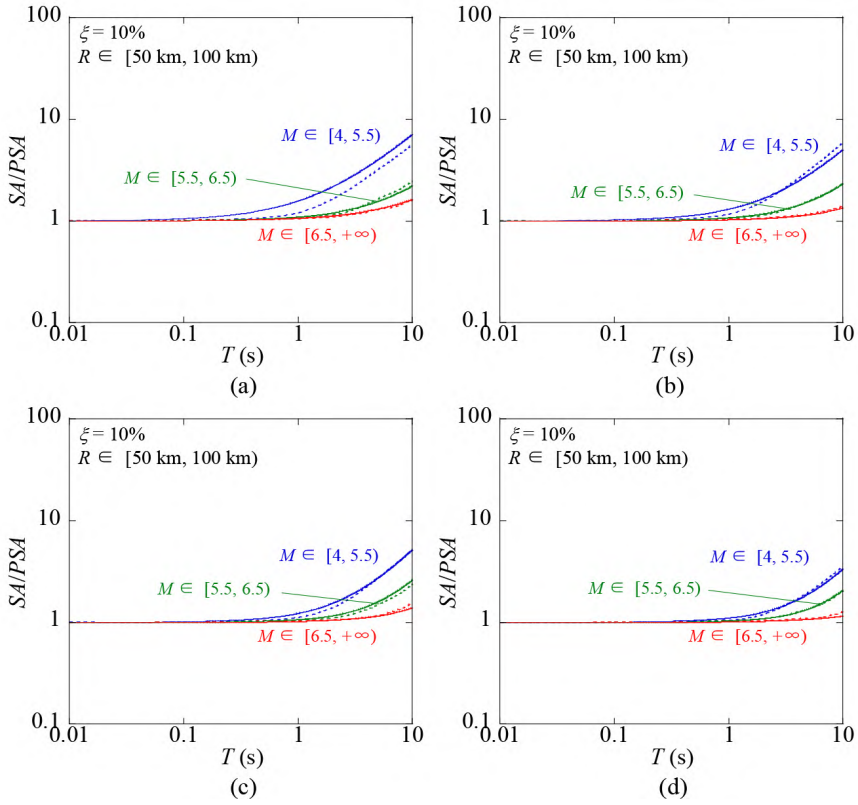

Fig. 6 Comparison of the *SA*/*PSA* results obtained by the proposed model and those obtained using the ground-motion database for model validation considering a damping ratio of 10% for (a) class B, (b) class C, (c) class D, and (d) class E. The solid lines represent the results from the proposed approach; the dashed lines represent the results obtained using the ground-motion database for model validation

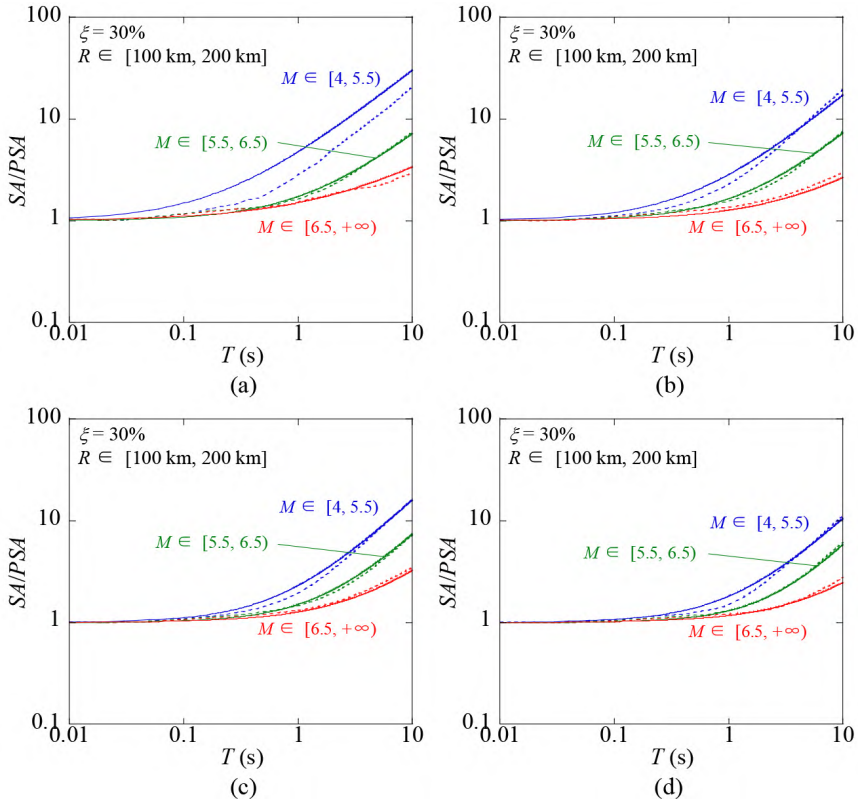

Fig. 7 Comparison of the *SA*/*PSA* results obtained by the proposed model and those obtained using the ground-motion database for model validation considering a damping ratio of 30% for (a) class B, (b) class C, (c) class D, and (d) class E. The solid lines represent the results from the proposed approach; the dashed lines represent the results obtained using the ground-motion database for model validation

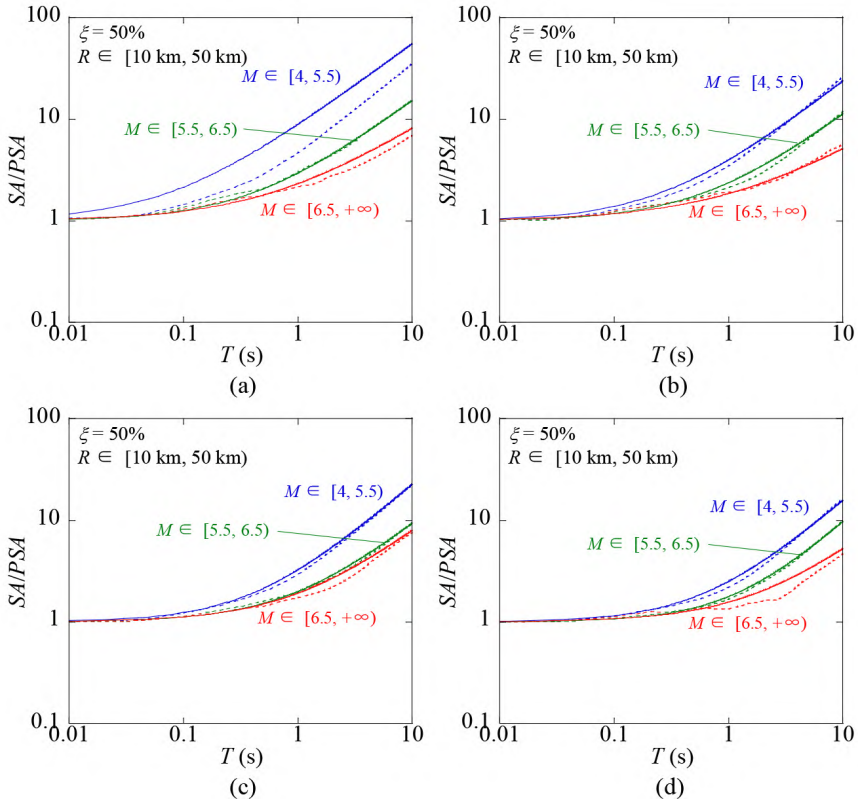

Fig. 8 Comparison of the *SA*/*PSA* results obtained by the proposed model and those obtained using the ground-motion database for model validation considering a damping ratio of 50% for (a) class B, (b) class C, (c) class D, and (d) class E. The solid lines represent the results from the proposed approach; the dashed lines represent the results obtained using the ground-motion database for model validation

between the *SA*/*PSA* results of the proposed model and those using seismic records is generally good. Although the accuracy of the proposed model decreases for cases with small magnitudes in site class B, it demonstrates similar accuracy for most cases compared to the results listed in Figs. 3–5. Similar trends were observed for results with damping ratios of 5%, 20%, and 40%, although these are not displayed here.

5 Comparison with existing models

The *SA*/*PSA* results obtained using the proposed model were compared with those of the existing models, including those from Sadek *et al*. (2000), Song *et al*. (2007), Mentristi (2008), Papagiannopoulos *et al*. (2013), Zhang and Zhao (2022b), and Hang *et al*. (2022), as well as those based on the database listed in Table 1. Some representative comparisons of *SA*/*PSA* are shown in Figs. 9–20. Figures 9–11 show the results of 10%, 30%, and 50% damping ratios for site class B, respectively. Figures 12–14 show the results of 10%, 30%, and 50% damping ratios for site class C, respectively. Figures 15–17 show the results of 10%, 30%, and 50% damping ratios for site class D, respectively. Figures 18–20 show the results of 10%, 30%, and 50% damping ratios for

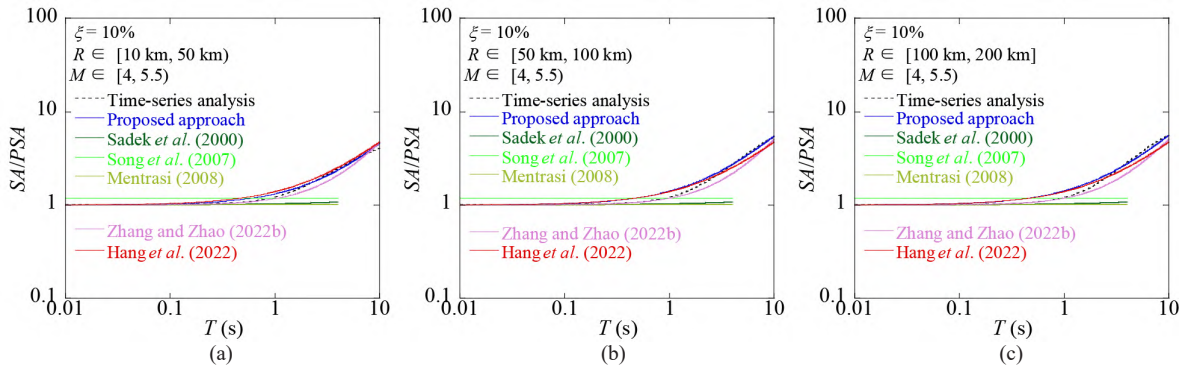

Fig. 9 Comparison of the *SA*/*PSA* results obtained by the proposed and existing models based on the database listed in Table 1 considering a damping ratio of 10% in class B for distances of (a) *R* ∈ [10 km, 50 km), (b) *R* ∈ [50 km, 100 km), (c) *R* ∈ [100 km, 200 km]

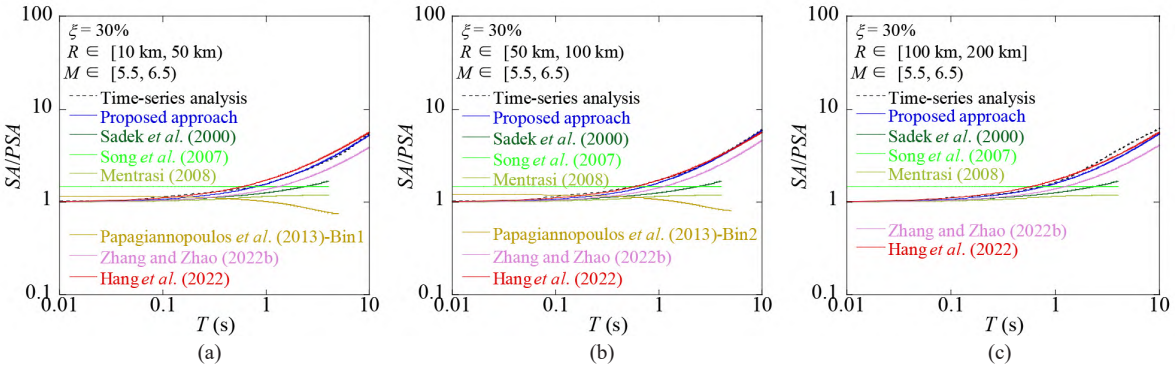

Fig. 10 Comparison of the *SA*/*PSA* results obtained by the proposed and existing models based on the database listed in Table 1 considering a damping ratio of 30% in class B for distances of (a) $R \in$ [10 km, 50 km), (b) $R \in$ [50 km, 100 km), (c) $R \in$ [100 km, 200 km]

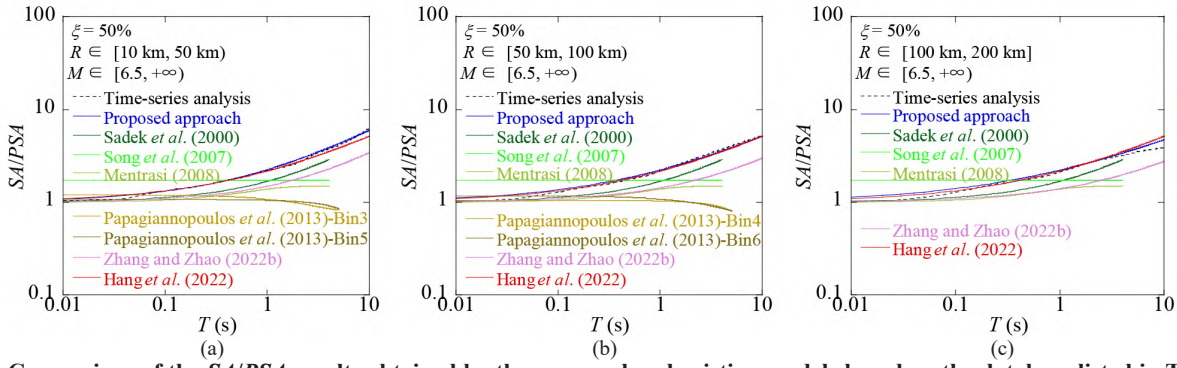

Fig. 11 Comparison of the *SA*/*PSA* results obtained by the proposed and existing models based on the database listed in Table 1 considering a damping ratio of 50% in class B for distances of (a) $R \in$ [10 km, 50 km), (b) $R \in$ [50 km, 100 km), (c) $R \in$ [100 km, 200 km]

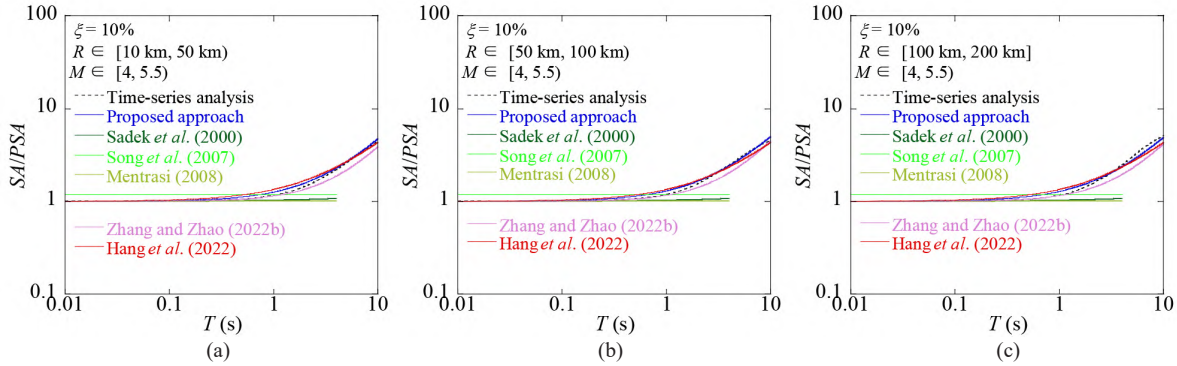

Fig. 12 Comparison of the *SA*/*PSA* results obtained by the proposed and existing models based on the database listed in Table 1 considering a damping ratio of 10% in class C for distances of (a) $R \in$ [10 km, 50 km), (b) $R \in$ [50 km, 100 km), (c) $R \in$ [100 km, 200 km]

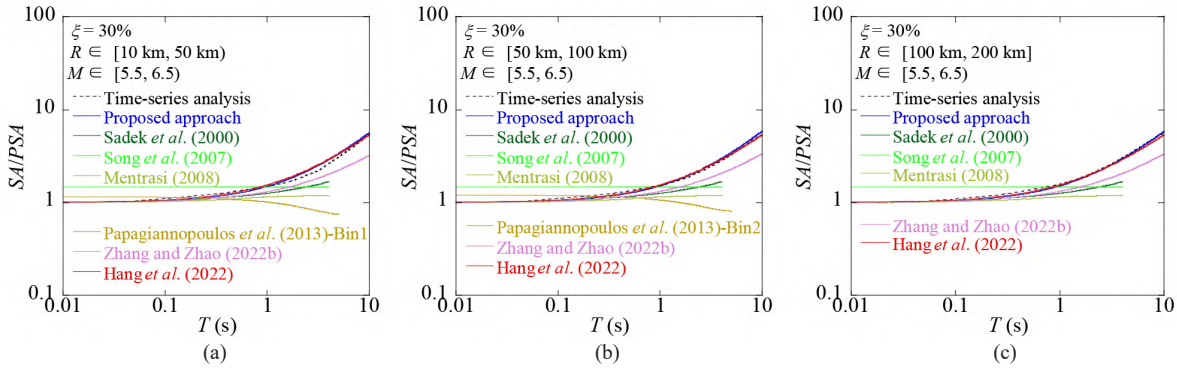

Fig. 13 Comparison of the *SA*/*PSA* results obtained by the proposed and existing models based on the database listed in Table 1 considering a damping ratio of 30% in class C for distances of (a) $R \in$ [10 km, 50 km), (b) $R \in$ [50 km, 100 km), (c) $R \in$ [100 km, 200 km]

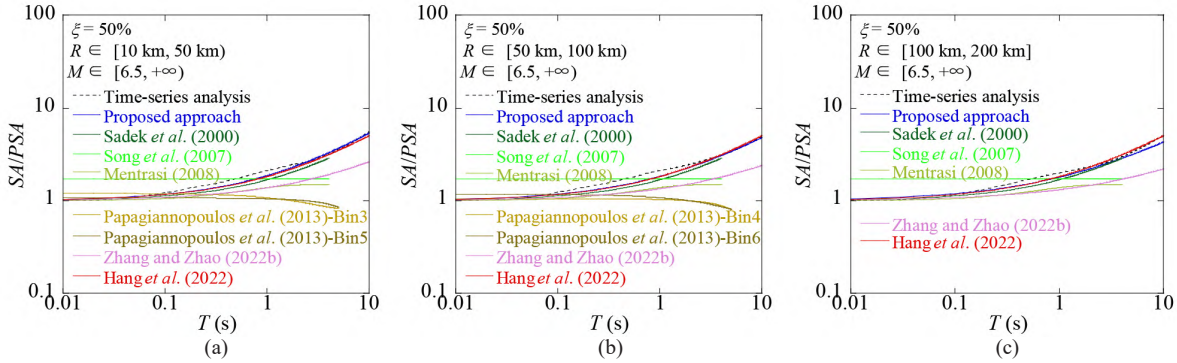

Fig. 14 Comparison of the *SA*/*PSA* results obtained by the proposed and existing models based on the database listed in Table 1 considering a damping ratio of 50% in class C for distances of (a) $R \in$ [10 km, 50 km), (b) $R \in$ [50 km, 100 km), (c) $R \in$ [100 km, 200 km]

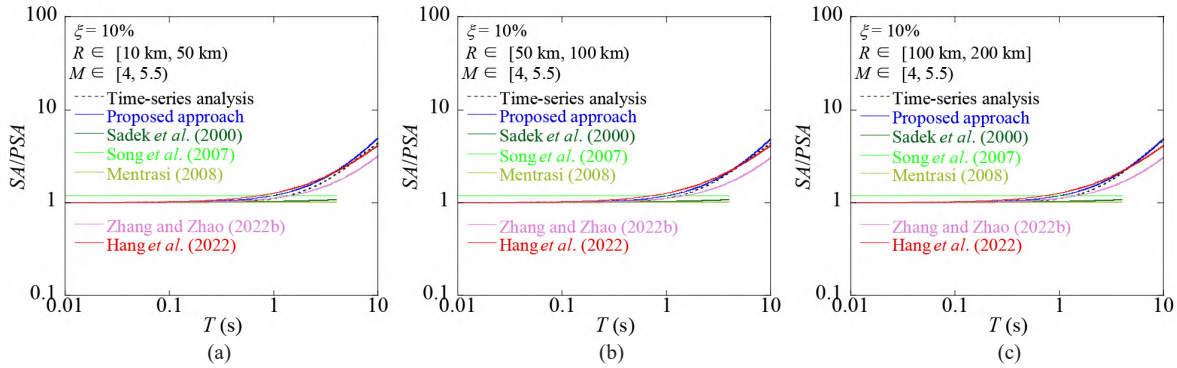

Fig. 15 Comparison of the *SA*/*PSA* results obtained by the proposed and existing models based on the database listed in Table 1 considering a damping ratio of 10% in class D for distances of (a) $R \in$ [10 km, 50 km), (b) $R \in$ [50 km, 100 km), (c) $R \in$ [100 km, 200 km]

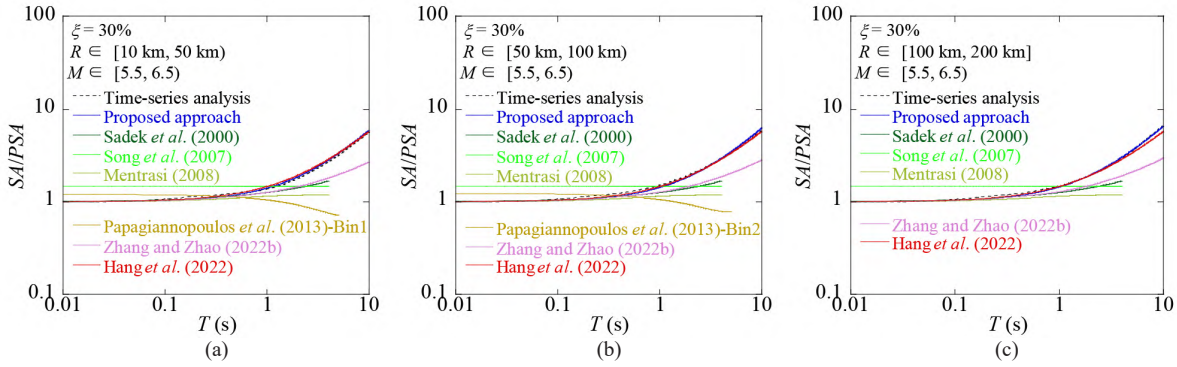

Fig. 16 Comparison of the *SA*/*PSA* results obtained by the proposed and existing models based on the database listed in Table 1 considering a damping ratio of 30% in class D for distances of (a) $R \in$ [10 km, 50 km), (b) $R \in$ [50 km, 100 km), (c) $R \in$ [100 km, 200 km]

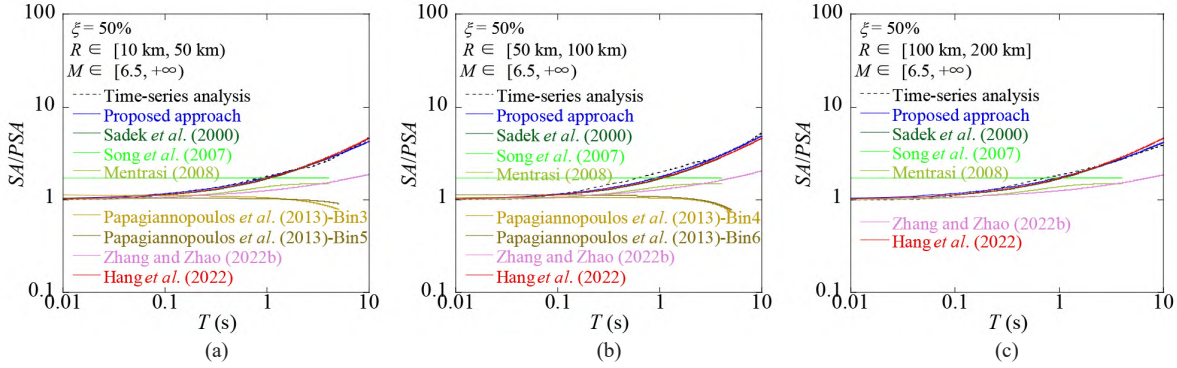

Fig. 17 Comparison of the *SA*/*PSA* results obtained by the proposed and existing models based on the database listed in Table 1 considering a damping ratio of 50% in class D for distances of (a) $R \in$ [10 km, 50 km), (b) $R \in$ [50 km, 100 km), (c) $R \in$ [100 km, 200 km]

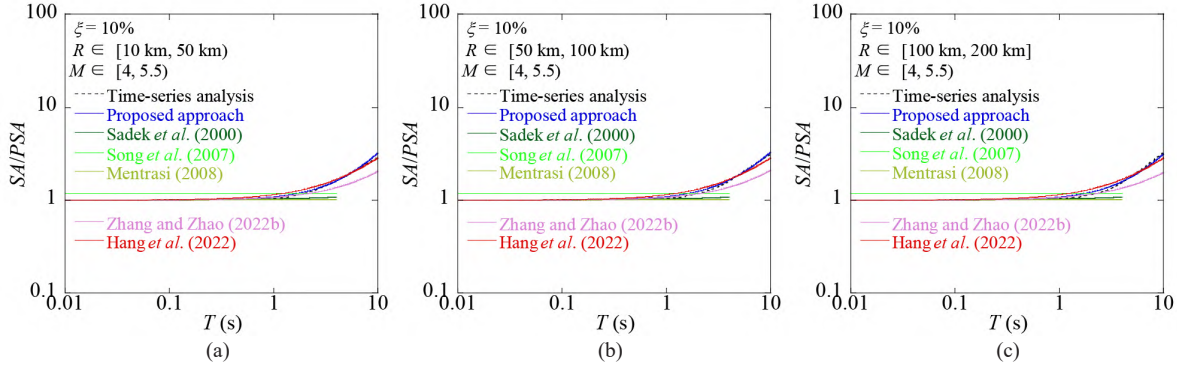

Fig. 18 Comparison of the *SA*/*PSA* results obtained by the proposed and existing models considering a damping ratio of 10% in class E for distances of (a) $R \in$ [10 km, 50 km), (b) $R \in$ [50 km, 100 km), (c) $R \in$ [100 km, 200 km]

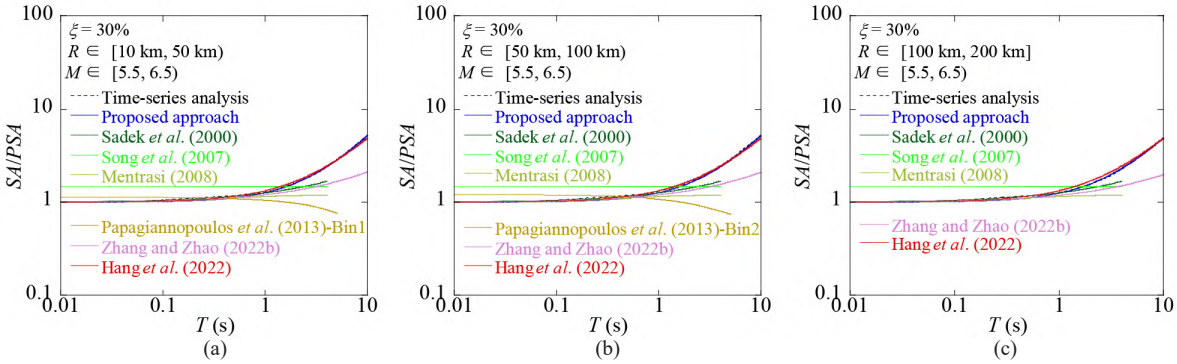

Fig. 19 Comparison of the *SA*/*PSA* results obtained by the proposed and existing models based on the database listed in Table 1 considering a damping ratio of 30% in class E for distances of (a) $R \in$ [10 km, 50 km), (b) $R \in$ [50 km, 100 km), (c) $R \in$ [100 km, 200 km]

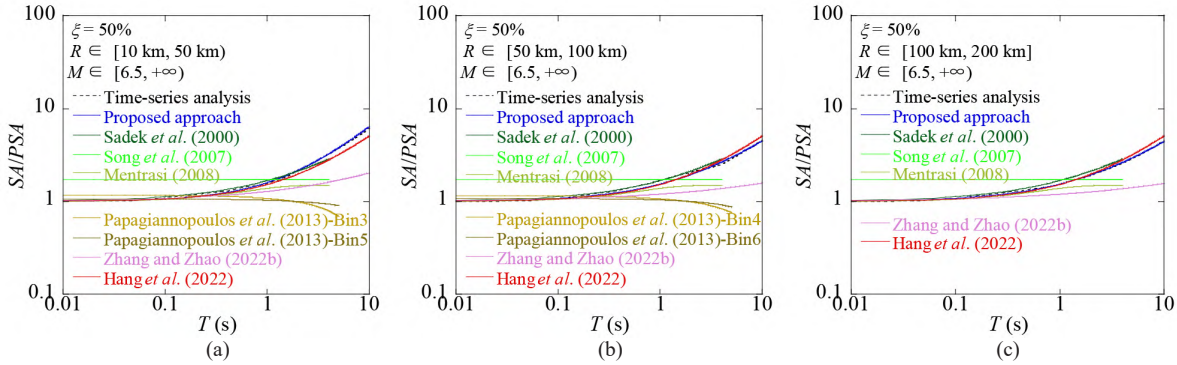

Fig. 20 Comparison of the *SA*/*PSA* results obtained by the proposed and existing models based on the database listed in Table 1 considering a damping ratio of 50% in class E for distances of (a) $R \in$ [10 km, 50 km), (b) $R \in$ [50 km, 100 km), (c) $R \in$ [100 km, 200 km]

site class E, respectively. Figures 9, 12, 15, and 18 do not include the results of the Papagiannopoulos model (Papagiannopoulos *et al*., 2013) because this model does not apply to cases in which the magnitude is less than six. Figures 10(c), 11(c), 13(c), 14(c), 16(c), 17(c), 19(c), and 20(c) do not include the results of the Papagiannopoulos model (Papagiannopoulos *et al*., 2013) because this model does not apply to cases in which the distance is larger than 100 km.

The accuracies of the *SA*/*PSA* results obtained by the models of Sadek *et al*. (2000), Song *et al*. (2007), Mentristi (2008), and Papagiannopoulos *et al*. (2013) are relatively poor compared to the proposed model. The accuracy of the model of Zhang and Zhao (2022b) is nearer to that of the proposed model in cases of small or moderate magnitudes, small damping ratios, and site class B, but the accuracy of the Zhang and Zhao (2022b) model decreases with increases in magnitude and damping ratio, as well as a variation in site class from B to E. For the case shown in Fig. 11, the average relative errors of the Zhang and Zhao (2022b) model are 39.98%, 42.6%, and 35% in Figs. 11(a), 11(b) and 11(c), respectively, while the average relative errors of the proposed model are only 1.43%, 2.57%, and 10.12%, respectively. Moreover, it can be found that the model of Hang *et al*. (2022) demonstrates the best

performance among the existing models. Nevertheless, the proposed model performs better than the model of Hang *et al*. (2022), especially for cases with small or large magnitudes, small damping ratios, long periods, and soft sites. The proposed model has fewer relative errors than the Hang model for 75.9% of the cases in site class B, 57.4% of the cases in site class C, 59.3% of the cases in site class D, and 79.6% of the cases in site class E. In addition, the proposed model demonstrates broader applicability compared to the model of Hang *et al*. (2022). Moreover, the model of Hang *et al*. (2022) cannot reflect the influence of distance, while the proposed model does.

The above comparisons with existing models are based on the database listed in Table 1. Similarly, comparisons using the ground-motion database for model validation (Table 2) were also conducted. Representative comparisons are shown in Figs. 21–23. By comparing Figs. 21–23 with Figs. 15–17, it is evident that the conclusions derived from the database provided in Table 1 are still validated when using the ground-motion database listed in Table 2.

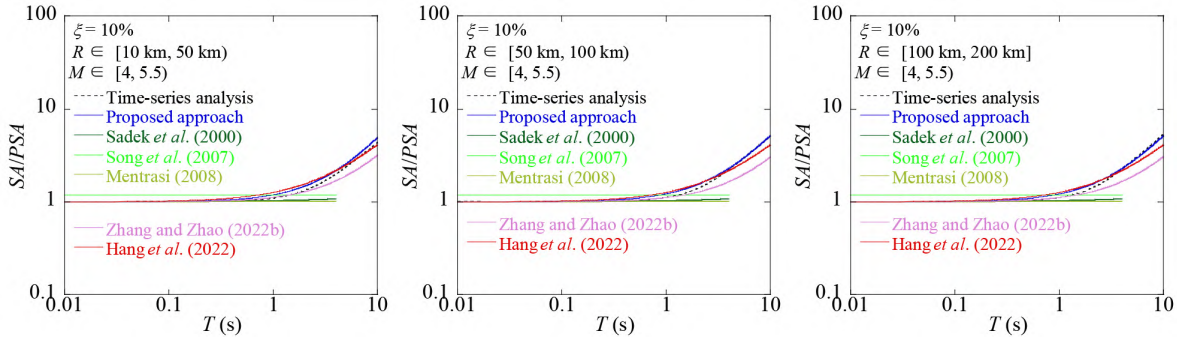

Fig. 21 Comparison of the *SA*/*PSA* results obtained by the proposed and existing models based on the database listed in Table 2 considering a damping ratio of 10% in class D for distances of (a) $R \in$ [10 km, 50 km), (b) $R \in$ [50 km, 100 km), (c) $R \in$ [100 km, 200 km]

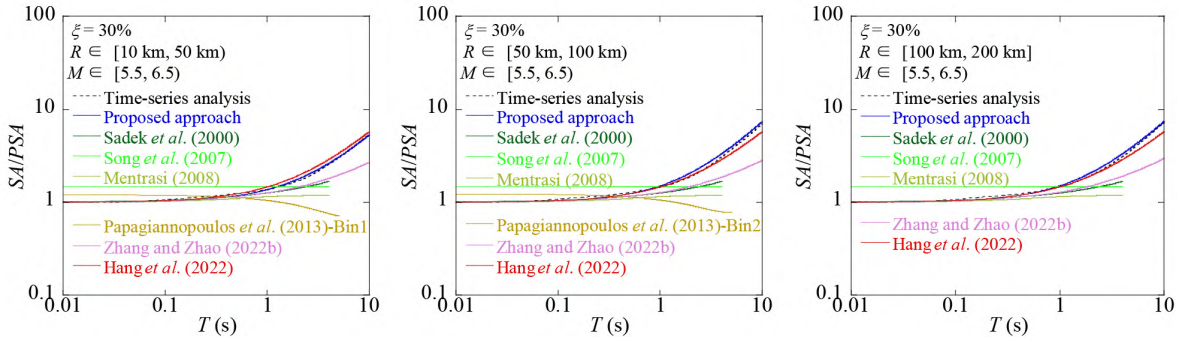

Fig. 22 Comparison of the *SA*/*PSA* results obtained by the proposed and existing models based on the database listed in Table 2 considering a damping ratio of 30% in class D for distances of (a) $R \in$ [10 km, 50 km), (b) $R \in$ [50 km, 100 km), (c) $R \in$ [100 km, 200 km]

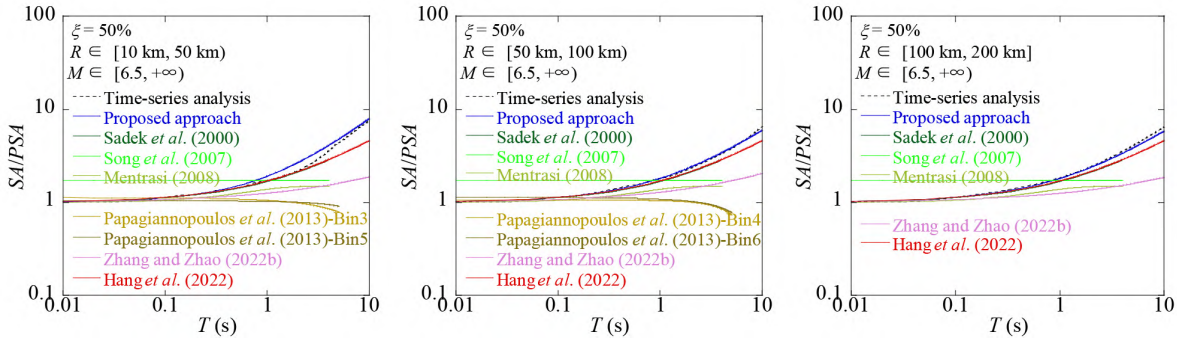

Fig. 23 Comparison of the *SA*/*PSA* results obtained by the proposed and existing models based on the database listed in Table 2 considering a damping ratio of 50% in class D for distances of (a) $R \in$ [10 km, 50 km), (b) $R \in$ [50 km, 100 km), (c) $R \in$ [100 km, 200 km]

6 Conclusions

This paper developed an efficient conversion model between the acceleration response spectrum (*SA*) and the pseudo-acceleration response spectrum (*PSA*) by considering influences of magnitude, distance, and site class. The proposed model can be applied to cases not only with small and moderate magnitudes but also with large magnitudes, which effectively realize the rationality of *SA* and *PSA* conversion and enhance its applicability in seismic design. The main conclusions of this study are summarized as follows.

(1) The *SA*/*PSA* results of the proposed model agree very well with those of seismic records; the accuracy of the proposed model increases with an increase in magnitude and increases as the site class varies from B to E.

(2) The accuracy of the model of Zhang and Zhao (2022b) is near to that of the proposed model in cases of small and moderate magnitudes, small damping ratios, and site class B, but the accuracy of the Zhang and Zhao (2022b) model decreases with increases of magnitude and damping ratio, and a variation in site class from B to E.

(3) The model of Hang *et al*. (2022) demonstrates the best performance among the existing models. Nevertheless, the proposed model performs better than the model of Hang *et al*. (2022), especially for cases with small or large magnitudes, small damping ratios, long periods, and soft sites. The proposed model has fewer relative errors than the Hang model for 75.9% of the cases in site class B, 57.4% of the cases in site class C, 59.3% of the cases in site class D, and 79.6% of the cases in site class E. In addition, the proposed model demonstrates broader applicability compared to the model of Hang *et al*. (2022). Moreover, the model of Hang *et al*. (2022) cannot reflect the influence of distance, while the proposed model does.

Acknowledgment

This study was partially supported by the National Natural Science Foundation of China (Grant No. 52278135). This study used strong-motion records from K-NET and KiK-net. The authors are grateful for the financial support and earthquake data.

References

Aoi S, Kunugi T, Nakamura H and Fujiwara H (2011), "Deployment of New Strong Motion Seismographs of K-NET and Kik-Net," in S Akkar, P Gülkan and T van Eck, editors, *Earthquake Data in Engineering Seismology: Predictive Models, Data Management and Networks*, Dordrecht: Springer, Netherlands, pp. 167–186.

ASCE/SEI 7-16 (2016), *Minimum Design Loads for Buildings and Other Structures*, American Society of Civil Engineers, Reston, USA.

Bahrampouri M, Rodriguez-Marek A, Shahi S and Dawood H (2021), "An Updated Database for Ground Motion Parameters for KiK-Net Records," *Earthquake Spectra*, **37**(1): 505–522.

Boore DM (2001), *Comparison of AA, PA and RV, PV for M_L = 4.5 and 7.1 Earthquakes*, http://daveboore.com/daves_notes/aa_pa_rv_pv_2.pdf.

BSL (2005), *Notification No. 631 of the Ministry of Land, Infrastructure, Transport and Tourism. Earthquake-Resistant Structural Calculation Based on Energy Balance*, Tokyo, Japan.

Chopra AK (2007), "Elastic Response Spectrum: A Historical Note," *Earthquake Engineering & Structural Dynamics*, **36**(1): 3–12.

Chopra AK and Chintanapakdee C (2001), "Comparing Response of SDF Systems to Near-Fault and Far-Fault Earthquake Motions in the Context of Spectral Regions," *Earthquake Engineering & Structural Dynamics*, **30**(12): 1769–1789.

Eurocode 8 (2010), *Design of Structures for Earthquake Resistance - Part 1: General Rules, Seismic Actions and Rules for Buildings*, Brussels: European Committee for Standardization, Belgium.

Fu J, Wang D, Zhang R and Chen X (2023), "Selection and Modification of Ground Motion Records Using Newmark-Hall Spectrum as Target Spectrum for Long-Period Structures," *Earthquake Engineering and Engineering Vibration*, **22**(1): 117–134.

GB 50010-2010 (2016), *Code for Design of Concrete Structures*, Beijing: China Architecture and Building Press, China. (in Chinese)

Hang BJ, Zhang HZ and Zhao YG (2022), "Effects of Magnitude, Epicentral Distance and Site Class on the Relationship Between Spectral and Pseudo-Spectral Acceleration," *Earthquake Engineering and Engineering Dynamics*, **42**(4): 48–57. (in Chinese).

Hatzigeorgiou GD (2010), "Damping Modification Factors for SDOF Systems Subjected to Near-Fault, Far-Fault and Artificial Earthquakes," *Earthquake Engineering & Structural Dynamics*, **39**(11): 1239–1258.

Jenschke VA, Clough RW and Penzien J (1964), "Analysis of Earth Motion Accelerograms," *Report No. SESM 64–1*, University of California, Berkeley, USA.

Jenschke VA, Clough RW and Penzien J (1965), "Characteristics of Strong Ground Motions," *Proceedings of the Third World Conference on Earthquake Engineering III, New Zealand*, 125–142.

Kalkan E (2016), "An Automatic P-Phase Arrival-Time Picker," *Bulletin of the Seismological Society of America*, **106**(3): 971–986.

Kanno T, Narita A, Morikawa N, Fujiwara H and Fukushima Y (2006), "A New Attenuation Relation for

Strong Ground Motion in Japan Based on Recorded Data," *Bulletin of the Seismological Society of America*, **96**(3): 879–897.

Lin YY and Chang KC (2003), "Study on Damping Reduction Factor for Buildings Under Earthquake Ground Motions," *Journal of Structural Engineering*, **129**(2): 206–214.

Mentrasti L (2008), "Estimate of Spectral and Pseudo-Spectral Acceleration Proximity," *Engineering Structures*, **30**(9): 2338–2346.

NEHRP (2000), *Recommended Provisions for Seismic Regulations for New Buildings and Other Structures*, Washington DC: Federal Emergency Management Agency, USA.

Newmark NM and Rosenblueth E (1971), *Fundamentals of Earthquake Engineering*, Englewood Cliffs: Prentice-Hall, USA.

Okada Y, Kasahara K, Hori S, Obara K, Sekiguchi S, Fujiwara H and Yamamoto A (2004), "Recent Progress of Seismic Observation Networks in Japan—Hi-Net, F-Net, K-NET and KiK-Net—," *Earthquake, Planets and Space*, **56**: xv-xxviii.

Papagiannopoulos GA, Hatzigeorgiou GD and Beskos DE (2013), "Recovery of Spectral Absolute Acceleration and Spectral Relative Velocity from Their Pseudo-Spectral Counterparts," *Earthquake Structures*, **4**(5): 489–508.

Sadek F, Mohraz B and Riley MA (2000), "Linear Static and Dynamic Procedures for Structures with Velocity-Dependent Dampers," *Journal of Structural Engineering*, **126**(8): 887–895.

Seyed Ardakani SM, Saiidi MS and Somerville P (2021), "Residual Drift Spectra for RC Bridge Columns Subjected to Near-Fault Earthquakes," *Earthquake Engineering and Engineering Vibration*, **20**(1): 193–211.

Song J, Chu YL, Liang Z and Lee GC (2007), "Estimation of Peak Relative Velocity and Peak Absolute Acceleration of Linear SDOF Systems," *Earthquake Engineering and Engineering Vibration*, **6**(2): 1–10.

Stewart JP, Chiou SJ, Bray JD, Graves RW, Somerville PG and Abrahamson NA (2002), "Ground Motion Evaluation Procedures for Performance-Based Design," *Soil Dynamics and Earthquake Engineering*, **22**(9–12): 765–772.

Veletsos AS and Newmark NM (1964), "Response Spectra for Single-Degree-of-Freedom Elastic and Inelastic Systems," *Report No. RTD-TDR-63–3096*, Vol. III, Air Force Weapons Laboratory, Albuquerque, USA.

Zhang D, Bai Y and Gao J (2016), "Probe into Several Important Concepts in Chinese Current Seismic Response Spectra," *Journal of Building Structures*, **37**(4): 110–118. (in Chinese)

Zhang HZ and Zhao YG (2022a), "Damping Modification Factor of Acceleration Response Spectrum Considering Seismological Effects," *Journal of Earthquake Engineering*, **26**(16): 8359–8382.

Zhang HZ and Zhao YG (2022b), "Effects of Magnitude and Distance on Spectral and Pseudospectral Acceleration Proximities for High Damping Ratio," *Bulletin of Earthquake Engineering*, **20**(8): 3715–3737.

Zhang HZ, Zhao YG, Ge FW, Fang YC and Ochiai T (2023), "Estimation of Input Energy Spectrum from Pseudo-Velocity Response Spectrum Incorporating the Influences of Magnitude, Distance, and Site Conditions," *Engineering Structures*, **274**: 115165.